

Communication

Piezotronic graphene barristor: Efficient and interactive modulation of Schottky barrier

Seongchan Kim^a, Young Jin Choi^a, Hwi Je Woo^a, Qijun Sun^{a,b,c,g,*}, Sungjoo Lee^a, Moon Sung Kang^d, Young Jae Song^a, Zhong Lin Wang^{b,c,e,g}, Jeong Ho Cho^{a,f,*}

^a SKKU Advanced Institute of Nanotechnology (SAINT), Sungkyunkwan University, Suwon 440-746, Republic of Korea

^b Beijing Institute of Nanoenergy and Nanosystems, Chinese Academy of Sciences, Beijing 100083, PR China

^c Center on Nanoenergy Research, School of Physical Science and Technology, Guangxi University, Nanning 530004, China

^d Department of Chemical Engineering, Soongsil University, Seoul 156-743, Republic of Korea

^e School of Materials Science and Engineering, Georgia Institute of Technology, Atlanta, GA 30332-0245, USA

^f School of Chemical Engineering, Sungkyunkwan University, Suwon, 440-746, Republic of Korea

^g School of Nanoscience and Technology, University of Chinese Academy of Sciences, Beijing 100049, PR China

ARTICLE INFO

Keywords:

Piezopotential modulation
Graphene barristor
Schottky barrier
Kelvin probe force microscopy
Interactive

ABSTRACT

The piezopotential generated in non-centrosymmetric crystals under external mechanical stimuli can be exploited to modulate the contact characteristics at the metal-semiconductor interface. The extent of electric modulation by the piezopotential was found to be moderate. This is mainly because the piezopotential was designed to alter the band bend of the semiconductor layer, which changed the injection barrier by 0.1 eV. We propose an efficient method to utilize the piezopotential for modulating Schottky barrier, i.e. piezotronic graphene barristor. This was done by capacitively coupling the piezoelectric material with a Schottky barrier (SB)-tunable graphene electrode, using an ion gel electrolyte. Through capacitive coupling, the piezopotential could modulate the work function of a graphene electrode by 0.89 eV. This was visualized directly using Kelvin probe force microscopy experiments for the first time. A large change in the work function of graphene allowed effective tuning of the height of the SB formed at the graphene/semiconductor junction. Consequently, a piezoelectric nanogenerator (PENG) could change the current density of the semiconductor layer by more than three orders of magnitude with strain, and yield a high current density larger than 10.5 A cm^{-2} . Multistage modulation of the height of the SB at the junction was also successfully demonstrated by integrating two PENGs with ion gel. This work presents an efficient method for harnessing the piezopotential generated from PENG to actively control the operation of flexible electronics through external mechanical stimuli.

1. Introduction

The piezoelectric effect originates from materials that lack inversion symmetry. This has received significant attention because it converts random mechanical energy including body movement, muscle stretching, and acoustic/ultrasonic waves directly to electricity [1–3]. The piezoelectric potential created in such materials, also known as piezoelectric nanogenerators (PENG), bridges the mechanical stimuli with various electronic devices such as transistors, diodes, strain/force/flow sensors, and electromechanical memories (i.e. piezotronic devices) [4–10]. Piezoelectric potentials, for instance, were utilized to gate transistors or generate programmed or erased states in memory devices through mechanical input, without applying electrical bias [11,12]. Recently, the piezopotential generated by wurtzite semiconducting

crystals like ZnO, GaN, InN, and ZnS has been coupled with the contact characteristics of electronic devices [13,14]. The junction properties at the metal-semiconductor (M-S) interface were tuned by the piezopotential. The contact characteristics at the M-S junction were modulated by both the magnitude and direction of the applied strain (compressive or tensile). Modification of the local band structure by creating a piezopotential at the p-n junction can enhance the mobility of charge carriers moving toward the junction and the electron-hole recombination rate in light-emitting diodes [15–17]. When using conventional metals as electrodes, the extent of piezopotential-induced modulations remains moderate. This happens because the generated piezopotential has limited influence on the band-bending characteristics of the semiconductor at the M-S junction. Therefore, an alternative strategy for the effective modulation of junction properties is required for practical

* Corresponding authors at: SKKU Advanced Institute of Nanotechnology (SAINT), Sungkyunkwan University, Suwon 440-746, Republic of Korea.
E-mail addresses: sunqijun@binn.cas.cn (Q. Sun), jhcho94@skku.edu (J.H. Cho).

device applications.

Graphene has attracted significant attention as a potential electronic material for future electronic devices due to its unique electrical, optical, and mechanical properties [18–23]. The work function of graphene is readily modulated by electric fields due to the linear energy dispersion relationship near the charge neutrality point in its band structure [24,25]. The ability to modulate the work function of graphene is the key feature in tuning the height of the Schottky barrier (SB) formed between graphene and the semiconductor [26–28]. If the piezopotential generated from PENG could be coupled with the graphene-semiconductor junction, this may serve as a more efficient way of harnessing the piezoelectric effect in electronic devices. This is because current injection at the electrode/semiconductor junction would vary when the SB height is altered beyond what can be achieved by changing the band-bending characteristics alone. The challenge is to then couple the piezopotential of PENG with the graphene electrode of an electronic device to form a SB with a contacting semiconductor.

In this work, we proposed a more efficient way of utilizing the piezopotential for modulating Schottky barrier, i.e. piezotronic graphene barristor. This was done by capacitively coupling the piezoelectric material with a monolayer graphene electrode via an ultrahigh capacitance ion gel electrolyte [29–32]. Through capacitive coupling, the piezopotential from a poly[vinylidene fluoride-co-trifluoroethylene] [P(VDF-TrFE)] PENG could modulate the work function of a graphene electrode by 0.89 eV, which was visualized directly using Kelvin probe force microscopy (KPFM) analysis for the first time. Such a large strain-induced change in the work function could change the current density of a vertical graphene-indium gallium zinc oxide (IGZO)-indium tin oxide (ITO) device by more than three orders of magnitude and yield a high current density larger than 10.5 A cm^{-2} . Interactive dynamic tests were also conducted, representing stable operation of the piezotronic graphene barristor. In addition, the multistep modulation of the SB formed at the junction was successfully demonstrated by connecting two PENGs to graphene through an ion gel. We consider that the demonstrated piezopotential-modulated graphene barristor constitutes a significant advancement in the development of micro-sensory systems, human-robot interactive interfaces, and transducers, which are crucial to the Internet of Things (IoT).

2. Results and discussion

Fig. 1a shows a schematic illustration of the surface potential measurements for monolayer graphene (Fig. S1) gated by piezopotential through an ion gel electrolyte. The surface potential of graphene modulated by a piezopotential (generated by the P(VDF-TrFE) PENG) was measured using KPFM [24,33]. This was compared with voltage-controlled modulation. KPFM is a nondestructive technique to observe the surface potential distribution without perturbations due to the absence of contact between the probe and the graphene surface [34,35]. As shown in Fig. 1a, the bottom ITO electrode of the piezoelectric nanogenerator (PENG) was extended to apply a piezopotential to graphene through the ion gel deposited inside the polydimethylsiloxane (PDMS) wall. The PDMS wall was utilized to easily transfer the graphene onto the ion gel and to deposit the Al contact.

As a KPFM measurement is principally based on electrostatic force microscopy (EFM) with additional DC-nulling feedback, a DC bias (V_{DC}) summed with an AC modulation voltage with frequency (ω) and amplitude (V_{AC}) was applied between the conductive probe and the sample to obtain the electrostatic field gradient [36,37]. The voltage applied between the probe and the local sample is then $V = (V_{DC} - V_{CPD}) + V_{AC} \sin(\omega t)$, where V_{CPD} is the contact potential difference (CPD). The electrostatic force between the probe and the sample can be induced from the spatial gradient (vertical direction or z axis) of capacitive energy ($1/2CV^2$) as follows.

$$F_z = -\frac{1}{2} \frac{\partial C}{\partial z} [(V_{DC} - V_{CPD}) + V_{AC} \sin(\omega t)]^2$$

This electrostatic force on the probe has three spectral components of the 0th order (constant in frequency), ω , and 2ω terms. The 0th order ($F_0 = \frac{\partial C}{\partial z} (\frac{1}{2}(V_{DC} - V_{CPD})^2 + \frac{1}{4}V_{AC}^2)$) and 2ω ($F_{2\omega} = \frac{1}{4} \frac{\partial C}{\partial z} V_{AC}^2 \cos(2\omega t)$) terms contribute to the topology and capacitance signals, respectively. The surface potential variation can be measured by mapping V_{DC} which is adjusted to null out the 1st order term ($F_\omega = -\frac{\partial C}{\partial z} (V_{DC} - V_{CPD}) V_{AC} \sin(\omega t)$).

Fig. 1b shows the KPFM images and histograms of the surface potentials (V_{CPD}) for monolayer graphene under different compressive and tensile strains applied to the PENG. The surface potential of graphene was measured to be $+0.22 \text{ V}$ under no external strain. As the

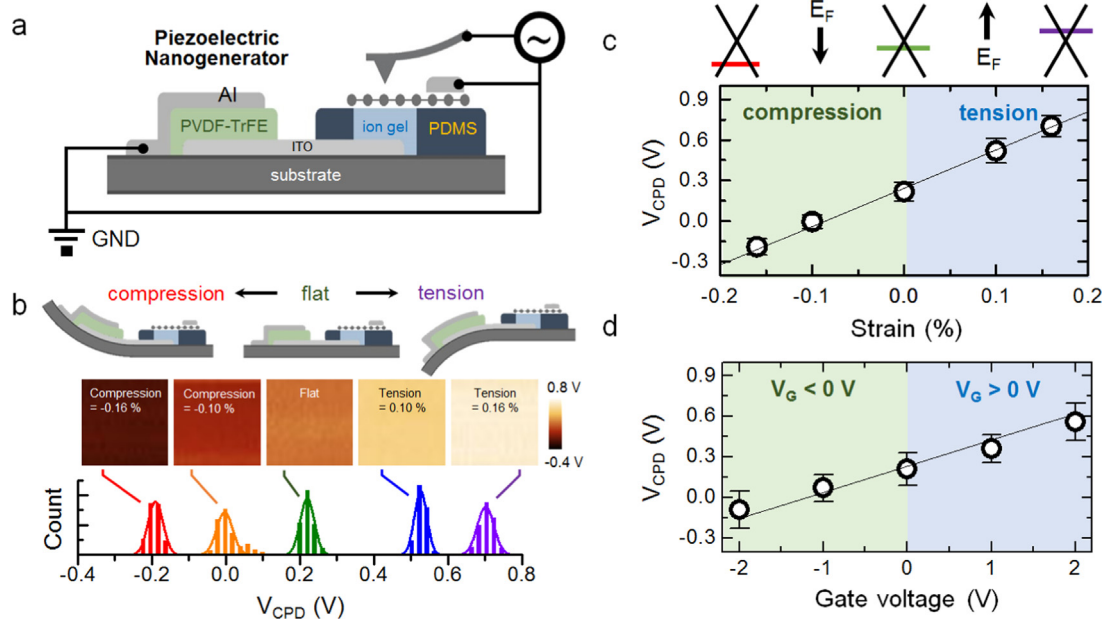


Fig. 1. (a) Schematic of the experimental setup for KPFM measurement. (b) KPFM images and histograms of the surface potentials for monolayer graphene at different compressive and tensile strains applied to the PENG. The upper panel shows a schematic of the KPFM samples upon applying strains. (c-d) Surface potential as a function of the applied strain (c) and voltage (d).

compressive strain increased to -0.16% , the surface potential reduced to -0.19 V. In contrast, when the tensile strain increased to $+0.16\%$, the surface potential increased to $+0.70$ V. The Gaussian fit distributions for the surface potentials of graphene under specific strains are illustrated in the lower panel of Fig. 1b. The piezopotential-induced variation of the surface potentials reflected the modulation of work functions based on the Fermi level (E_F) shift of graphene (Fig. 1c). When the external strain was varied from -0.16% (compression) to 0.16% (tension), the modulation of the surface potential of graphene was as high as 0.89 V. The surface potential change according to relevant piezopotential under applied strains (from -0.16% to 0.16%) is shown in Fig. S2, representing a linear increment *versus* piezopotential. The relation between the V_{CPD} and work function of graphene can be expressed as $eV_{CPD} = W_{probe} - W_{graphene}$, where W_{probe} and $W_{graphene}$ are the work functions of the probe and graphene, respectively [24]. As the piezopotential cannot influence the local surface potential at the probe apex, the above equation can be reduced to $\Delta W_{graphene} = -eV_{CPD}$, where $\Delta W_{graphene}$ and ΔV_{CPD} are changes to the work function of graphene and the measured surface potential under external strain, respectively. Therefore, the variation of the work function of graphene due to the piezopotential was estimated to be 0.89 eV. This value was comparable with the variation in the work function under application of voltages between -2 V and 2 V, where the DC voltage was applied to the ITO electrode (without applying external strains) while conducting the KPFM measurement (Fig. 1d and S3). The surface potential exhibited a gradual increase with a positive increase in the voltage due to the upward shift of the E_F for graphene. The piezopotential modulation of the graphene work function indicated that the piezopotential produced by the PENG can be utilized to control charge injection from the electrode to the semiconductor.

The deterministic piezopotential modulation of the graphene work function by external strain can be directly linked to the electronic device utilizing this property. The operation of the graphene barristor was based on modulation of the SB formed at the graphene-semiconductor heterostructure. The graphene barristor was integrated with the PENGs, i.e. piezotronic graphene barristor (illustrated in Fig. 2a). ITO patterns for the drain electrode, the contact pad for the graphene source electrode, and the extended coplanar gate (i.e. bottom electrode of NG) of the transistor were prepared by conventional photolithography and a subsequent acid etching processes. The IGZO precursor solution—comprising indium nitrate hydrate, gallium nitrate hydrate, and zinc acetate dehydrate dissolved in 2-methoxyethanol—was spin-coated onto the substrate with the patterned ITO electrodes. The IGZO layer was sintered through deep-UV irradiation to form an IGZO metal-oxide-metal network structure [38]. A vertical IGZO channel with a thickness of ~ 50 nm was formed by repeating the spin-coating and subsequent sintering processes four times. The semiconducting IGZO channel layer was also patterned using photolithography and chemical etching. The vertical IGZO channel was formed by transferring CVD-grown monolayer graphene on top of the IGZO pattern. The channel area was defined by the crossed area between the graphene source and ITO drain electrodes. The P(VDF-TrFE) layer was patterned onto the extended ITO gate electrode using a conformal polymeric mask [39]. The top Al electrode for the PENG was deposited through the shadow mask. Finally, the ion gel gate dielectric layer for the transistors was patterned to cover the IGZO channel and a portion of the ITO coplanar-gate electrode. The long-range polarizability of the ion gel enabled the gate electrode to be positioned in a coplanar structure with the channel layer and the drain electrode. Besides, ion gel was ionically conducting but electronically insulating, so the charges repelled by PENG piezopotential could not be neutralized through external circuit. When the strain was applied to PENG and remained fixed, the piezopotential-induced charges (including ions and electrons) redistributed and reached an equilibrium state, premising subsequent continuous piezopotential gating measurement. Fig. 2b shows the cross-sectional view of a schematic piezotronic graphene barristor (see the photographic device

image in Fig. S4). The piezopotential produced from P(VDF-TrFE) PENG under external strain was coupled with the graphene electrodes of the transistor through the ion gel. The formation of an electric double layer (EDL) at both the graphene-ion gel and ion gel-ITO interfaces resulted in ultrahigh capacitance [40], which allowed efficient modulation of the SB upon moderate output (< 5 V) of our PENG.

Piezopotential modulation of the SB formed at the graphene-IGZO junction by the PENG was first examined. In order to exclude the piezoresistive effect of IGZO channel and graphene layer, a custom linear motor controller for applying strain was fixed on the probe station (Fig. S5). The graphene barristor region was fully attached on the chuck, while the extended ITO gate with P(VDF-TrFE) NG was located off the chuck. The linear motor controller with a clamp was fixed on the end of P(VDF-TrFE) NG. Thus, the external strain was only applied on the NG region to make sure that no deformation occurred in the graphene barristor and affected the transistor operation. Fig. 2c shows the output characteristics [drain current (I_D) versus drain voltage (V_D)] of the piezopotential-modulated graphene barristor. Five different tensile or compressive strains were applied to the PENG and I_D was measured as a function of V_D while maintaining each strain. I_D was modulated effectively by varying the strain. Asymmetric current modulation was observed with the opposite polarity of V_D s. A larger modulation in the current level was observed under positive V_D compared to that of the negative V_D . Under positive V_D , I_D was dominated by the SB formed at the graphene-IGZO interface because electrons were injected from graphene to the IGZO channel. The compressive strain applied to the PENG generated a negative output voltage, which was delivered to the ITO coplanar gate electrodes of the transistors. The negative output voltage led to the accumulation of holes in the graphene source electrode and shifted the E_F of graphene downward due to the limited density of states of graphene. Thus, the electron injection barrier at the graphene-IGZO interface increased. In contrast, the tensile strain applied to the PENGs generated a positive output voltage. The resulting upward shift of the E_F of graphene reduced the electron injection barrier at the graphene-IGZO interface. The height of the SB formed at the graphene-IGZO interface was effectively modulated by the external strain applied to the PENG. For a negative V_D , I_D was affected mainly by the SB at the ITO-IGZO interface because electrons were injected from the metal to IGZO. Moderate current modulation was observed in this region. The fixed height of the electron injection barrier at the IGZO-ITO junction induced ineffective current modulation due to the high density of states (DOS) of the ITO electrode [28]. The piezopotential-induced asymmetric I_D modulation at opposite V_D s was similar to that under different gate voltages, V_{GS} (Fig. 2d) and was consistent with the results of KPFM. The detailed working mechanism of electrolyte gated graphene barristor is illustrated in Fig. S6. When a positive piezopotential was applied to the ITO gate, the anions in the electrolyte migrate toward the interface of the ITO and ion gel in order to compensate the charge build up in the gate electrode. According to the long range polarization of ion gel, the cations could move towards the ion-gel/graphene/IGZO interface and accumulated as a Helmholtz layer because they were blocked by the solid semiconductor. The accumulated cations played two important roles in the graphene barristor. One was that the cations attracted electrons to accumulate at the IGZO/graphene/ion-gel interface due to the weak electrostatic screening effect of graphene and lead to an enhancement in the output currents. The other role was to tune the work function of graphene and affect the SB formed between graphene and IGZO channel, leading to an asymmetric I_D modulation at opposite V_D s.

The piezopotential-induced SB modulation in the devices was also confirmed by the variation of I_D as a function of the applied strain. A tensile strain was applied to the PENG at a speed of 0.3 mm/s, and I_D was monitored under positive V_D s as a function of time (Fig. 2e). As the tensile strain increased with time, the higher positive output voltage (generated by the PENG) gradually shifted the E_F of graphene upward. The gradual reduction of the electron injection barrier at the graphene-

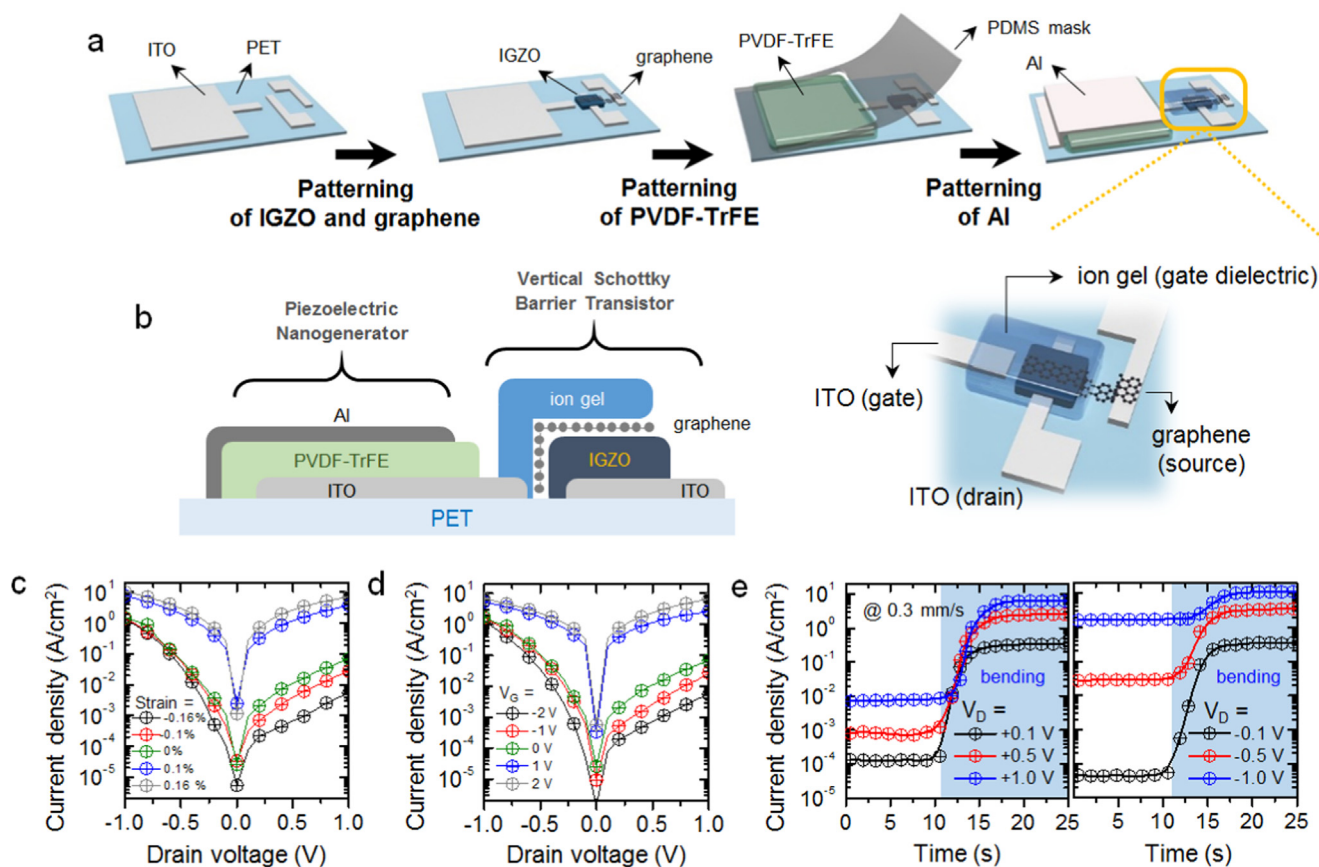


Fig. 2. (a) Schematic illustrating the steps for the fabrication of piezotronic graphene barristor. (b) Cross-sectional schematic of the device structure. (c-d) Plots of current density versus drain voltage at different strains (c) and gate voltages. (e) Plot of current density versus time during the application of tensile strain at a rate of 0.3 mm/s.

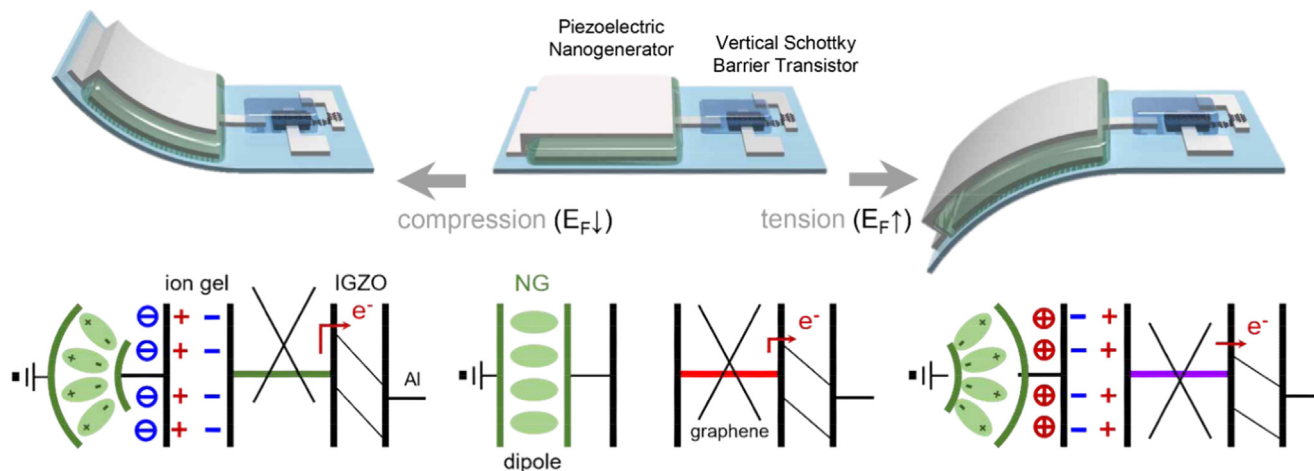


Fig. 3. Schematic band diagrams of the piezopotential-modulated SB formed at the graphene-IGZO junction through ion gel. Without external applied strain, the E_F of graphene was located near the Dirac point. Under compression, the induced negative piezopotential shifted the E_F of graphene downward and increased the electron injection barrier from graphene to IGZO. Under tension, the induced positive piezopotential shifted the E_F of graphene upward and decreased the electron injection barrier from graphene to IGZO.

IGZO interface increased the I_D of the device. In contrast, a moderate modulation of I_D was observed under negative V_D s due to ineffective SB modulation at the ITO-IGZO junction. The non-linear behavior of the current density as a function of time (strain) was observed and explained in details in Fig. S7. Before 7.5 s, no external strain was applied, the current density maintained at stable values (white region). When the tensile strain was applied to the device at 7.5 s, the drain current density represented no current modulation (blue region). In this region,

the drain current was limited by leakage and charging currents (i.e. the off-state of the graphene barristor). When the strain was gradually increased to the equivalent turn-on voltage of the graphene barristor ($\epsilon_{\text{turn-on}}$), the current density showed relevant increments in an exponential function (red region). After the applied strain continued to increase over the equivalent threshold voltage (ϵ_{th}) of the graphene barristor, a conducting path formed between the source and drain electrodes (i.e. the on-state of the graphene barristor, yellow region).

When the external strain was further increased (ϵ_{sat}), the piezopotential could not further influence the Fermi energy of the IGZO channel layer and the current density of the graphene barristor reached a saturation level (green region). Because the V_{OUT} of the PENG increased with time, one may expect the current of the device to increase with increasing gate potential with time. The increase was observed for only a limited period of time and the current became eventually saturated. The saturation could be attributed to the ineffective charge transport (mobility) at extremely large carrier densities where limited energy states were available for transport, which counter-balance each other. This behavior was observed in the graphene barristor operated by an applied gate bias (Fig. S8). Consequently, the SB at the graphene-IGZO junction was successfully modulated by the piezopotential upon application of strain.

The device operation can be understood in terms of the band diagrams shown in Fig. 3. As an example, we considered the application of positive V_{D} . Under compressive strain, the enhanced dipoles repel electrons to the interface between the ITO electrode and the ion gel. The cations in the ion gel migrated to this interface while the anions moved to the ion gel-graphene interface and the accumulated holes in graphene [11]. Due to the limited density of states in graphene, the E_{F} of graphene shifted downward and the electron injection barrier from graphene to IGZO increased. The tensile strain applied to the NG repelled holes to the ITO-ion gel interface and accumulated electrons in graphene. The SB height between graphene and IGZO decreased, which facilitated electron injection to the IGZO channel. The current density of the devices exhibited gradual increase with the increase in strain, varying from -0.16% (compression) to 0.16% (tension).

The piezopotential modulation of the height of the SB (ϕ_{B}) at the graphene-IGZO junction was quantitatively probed by temperature-dependent current-voltage measurements. According to the thermionic emission theory [26], the diode saturation current (I_{sat}) is related to ϕ_{B} by the equation $I_{\text{sat}} = AA^*T^2 \exp\left(-\frac{q\phi_{\text{B}}}{k_{\text{B}}T}\right)$, in which A is the junction area, A^* is the effective Richardson constant, q is the elementary charge, k_{B} is Boltzmann's constant, and T is the absolute temperature. I_{sat} , under a specific strain and temperature, was determined in the positive V_{D} regime where electrons were injected from graphene to IGZO. Fig. 4a shows the representative output curves measured at various temperatures ranging from 340 to 300 K at strains of 0 and $+0.16\%$. Curves were fitted in a linear fashion and the values of I_{sat} were defined to be at the points where the fitting lines crossed the y -axis. The values of ϕ_{B} for the graphene-IGZO junction were extracted from the slopes of the $\ln(I_{\text{sat}}/T^2)$ vs. $1/k_{\text{B}}T$ plots in Fig. 4b. ϕ_{B} varied from 1.07 to 0.15 eV as the external strain increased from -0.16% to 0.16% (Fig. 4c). Corresponding to the change in the work function of graphene, ϕ_{B} was effectively modulated by the piezopotential. ϕ_{B} was also characterized in the same way upon applying different V_{GS} (Fig. 4d–f), exhibiting a variation from 1.02 to 0.08 eV as V_{GS} increased from -2 to 2 V (see the band structure in Fig. S8c). The piezopotential-modulated ϕ_{B} was around 0.92 eV, which was comparable to that controlled by varying V_{G} (0.94 eV from -2 V to 2 V). The SB modulation observed in the device was consistent with the variation in the work function of graphene measured by KPFM (see Fig. 1).

The multistep modulation of SB at the graphene-IGZO junction was successfully demonstrated by integrating two PENGs to the graphene electrode through an ion gel (Fig. 5 and S9). The patterning of P(VDF-TrFE) using a polymeric stencil and the coplanar gate geometry of the graphene barristor both enabled facile integration of the graphene barristor and the two PENGs. The piezopotentials produced from the two PENGs were coupled with the graphene barristor through the single ion gel. When one PENG was subjected to an external tensile strain of 0.08% , the induced positive piezopotential led to the accumulation of electrons in graphene and shifted its E_{F} upward. When a tensile strain of 0.08% was applied to the other PENG, the corresponding piezopotential led to an even greater accumulation of electrons in graphene and

further shifted E_{F} upward (upper panel of Fig. 5). As the external strains were released sequentially, the E_{F} of graphene shifted downward stepwise without mutual interference. The lower panel of Fig. 5b shows stepwise variations in the output voltage of the PENGs (measured at the ITO gate electrode) and current density of the graphene barristor. Dynamic and long-term stability tests of the piezotronic graphene barristor were further conducted with varying tensile strains (Fig. S10, S11, and S12), demonstrating the strain-dependent stepwise modulation of the SB and its excellent operational robustness.

3. Conclusion

In conclusion, we demonstrated an efficient and interactive way to modulating Schottky barrier in piezotronic graphene-IGZO barristor. The resulting devices exhibited good electrical properties including a high current density of over 10.5 A cm^{-2} and a high on-off ratio of over 10^3 . Under external mechanical stimuli, the Schottky barrier height was significantly reduced by 0.89 eV in the piezopotential-modulated graphene barristor, which was also confirmed by KPFM and characterized by temperature-dependent transport measurements. Interactive multi-step SB modulation at the junction was successfully demonstrated by connecting two PENGs to the graphene electrode through an ion gel. The proposed piezotronic graphene barristor through high capacitive electrolyte coupling offers an efficient means for seamless and adaptive interactions between flexible functional devices and their surroundings (users or external mechanical stimuli). Further improvement on the modulation of Schottky barrier lays in optimization of the output efficiency of PENG, integration technics, structure of graphene barristor, contacts in graphene barristor, external temperature, etc.

4. Experiments

4.1. Material preparation

P(VDF-TrFE) (ARKEMA Inc.) (20 wt%) was dissolved in *N,N*-dimethylformamide (DMF), and then stirred for over 24 h. The ion gel solution was prepared by mixing poly(ethylene glycol) diacrylate (PEGDA) monomer, 2-hydroxy-2-methylpropiophenone (HOMPP) initiator, and 1-ethyl-3-methylimidazolium bis(trifluoromethanesulfonyl) imide ([EMIM][TFSI]) ionic liquid in the weight ratio 2:1:22. The IGZO precursor solution was prepared by dissolving 0.085 M of indium nitrate hydrate, 0.0125 M of gallium nitrate hydrate, and 0.0275 M of zinc acetate dehydrate in 10 mL of 2-methoxyethanol and then stirred at 75°C for 12 h.

4.2. Device fabrication

The piezopotential-modulated graphene barristor was prepared on a $200 \mu\text{m}$ -thick polyarylate (PAR) film (A200HC, Ferrania Technologies). A 40 nm -thick Al_2O_3 layer was deposited by atomic layer deposition (ALD) and a 50 nm -thick ITO layer was then deposited via RF magnetron sputtering. The ITO layer was patterned by photolithography (AZ 5214E) and chemical etching (35 vol% hydrochloric acid in water) to form the drain electrode, the contact pad for graphene source electrode, and the extended coplanar gate electrode. The sheet resistance of ITO was $45 \Omega/\text{sq}$. The IGZO layer was deposited by spin-coating (4000 rpm for 30 s) using the pre-prepared IGZO solution and dried at 60°C for 1 min. High-density deep-UV (wavelength = 253.7 and 184.9 nm) illumination was employed for 10 min in an N_2 environment. The spin-coating and subsequent sintering processes were repeated four times to form a thickness of 50 nm . The IGZO layer was patterned via photolithography and chemical etching [3 vol% LCE-12 (Cyantek Co.) in water]. The surface roughness of the IGZO film was around 0.9 nm (Fig. S13). The CVD-synthesized monolayer graphene was then transferred and patterned onto the IGZO channel by the previously reported method. The sheet resistance of monolayer graphene was $947 \Omega/\text{sq}$. The

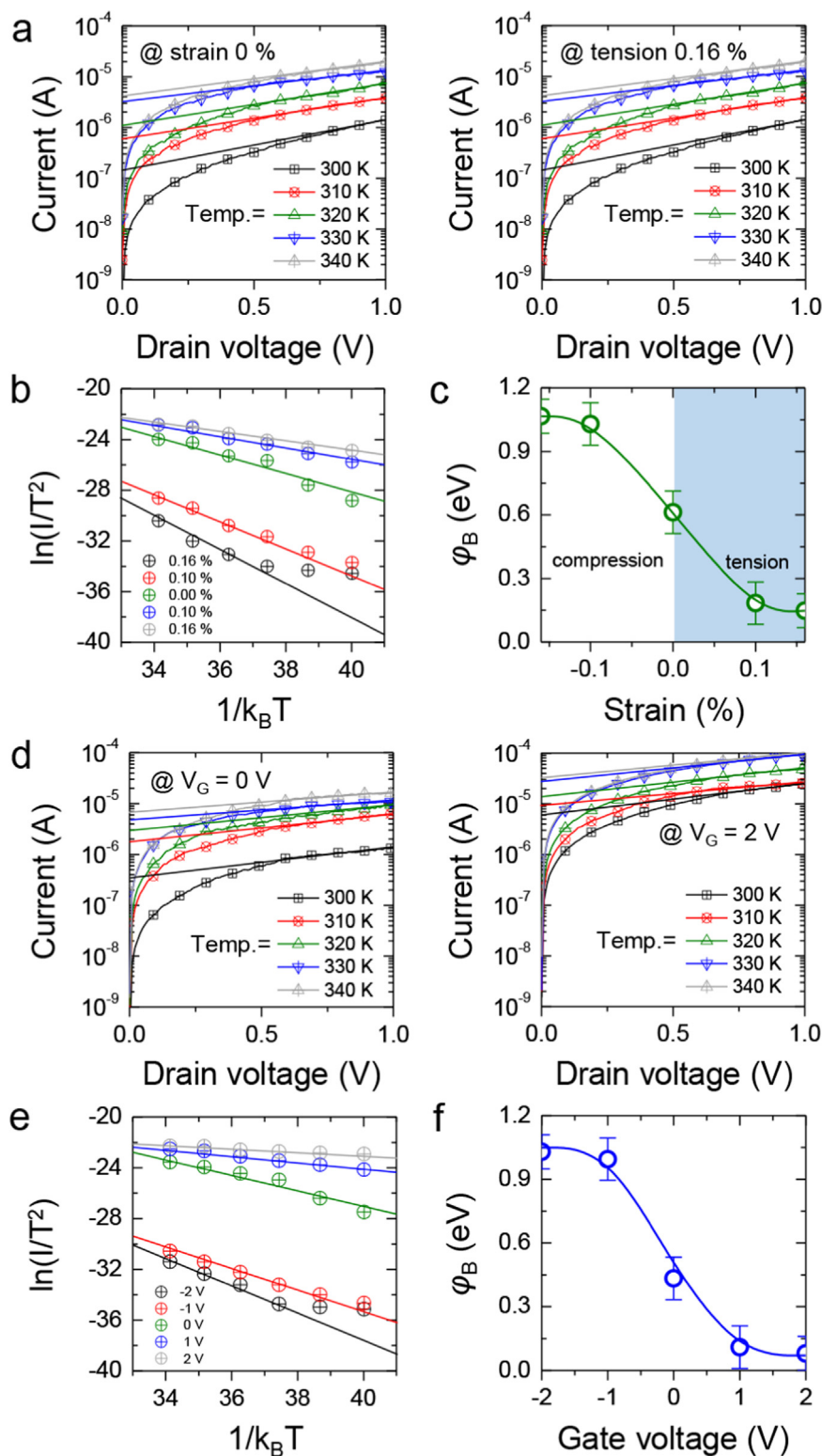


Fig. 4. (a) Representative output curves measured at temperatures ranging from 340 to 300 K and strains of 0 and +0.16%. (b) The plots of $\ln(I_{sat}/T^2)$ versus $1/k_B T$ under different applied strains. (c) Piezopotential-modulated SB heights at different strains. (d) Representative output curves measured at temperatures ranging from 340 to 300 K at $V_G = 0$ and 2 V. (e) Plots of $\ln(I_{sat}/T^2)$ versus $1/k_B T$ at different V_G s. (f) V_G -modulated SB heights at different V_G s.

P(VDF-TrFE) layer was patterned onto the extended ITO gate electrode using a polymeric mask and annealed at 140 °C for 3 h. The Al top electrode for the PENG was thermally deposited onto the P(VDF-TrFE) layer through a shadow mask. The P(VDF-TrFE) layer was then poled electrically. Finally, the ion gel consisting of a propylene glycol monomethyl ether acetate (PEG-DA) monomer, a 2-hydroxy-2-

methylpropiophenone (HOMPP) initiator, and an 1-ethyl-3-methylimidazolium bis(trifluoromethylsulfonyl) imide ([EMIM][TFSI]) ionic liquid (weight ratio of 2:1:22) was patterned via drop-casting and selective UV exposure.

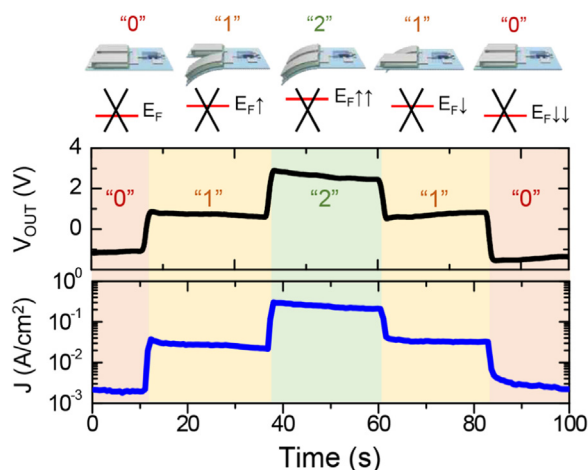


Fig. 5. Real-time multistage modulation of the current density in the graphene barristor under the output voltages generated by the two PENGs. The upper panel shows a schematic illustration of the multistage modulation of the height of the SB.

4.3. Characterization

KPFM measurement was conducted using a Park Systems NX10 AFM in ambient conditions. The electrical properties of the piezopotential-modulated graphene barristor were measured under nitrogen condition using a Keithley 4200. In order to prepare the samples for KPFM measurement, the PDMS layer with rectangular bank ($3 \times 3 \text{ mm}^2$ and height = 500 μm) was placed onto the ITO patterned substrate. The ion gel precursor was then drop-cast onto the void of PDMS bank and then exposed by UV. The CVD-grown single-layer graphene with $5 \times 5 \text{ mm}^2$ size was transferred onto the ion gel layer. The PMMA supporting layer was then removed using acetone within a short time < 10 s. The graphene larger than PDMS bank prevented the direct contact between the ion gel and the acetone to minimize the damage of underlying ion gel. The quality of monolayer graphene transferred onto the ion gel was confirmed by using AFM and Raman spectroscopy (Fig. S14).

Acknowledgements

Q. Sun was supported financially by the support of the National Key Research and Development Program of China (2016YFA0202703), National Natural Science Foundation of China (Grand nos. 51605034 and 51711540300), the “Hundred Talents Program” of the Chinese Academy of Science, and the “thousands talents” program for pioneer researcher and his innovation team. This work was also supported financially by a grant from the Center for Advanced Soft Electronics (CASE) under the Global Frontier Research Program (2013M3A6A5073177), the Basic Science Research Program through a National Research Foundation of Korea grant funded by the Korean Government (MEST) (2017R1A4A1015400), and the Pioneer Research Center Program (Grant no. 2014M3C1A3053024), Korea.

Appendix A. Supplementary material

Supplementary data associated with this article can be found in the online version at <http://dx.doi.org/10.1016/j.nanoen.2018.06.010>.

References

- [1] W.Z. Wu, Z.L. Wang, *Nat. Rev. Mater.* 1 (2016) 16031.
- [2] Z.L. Wang, *Adv. Mater.* 24 (2012) 4632–4646.
- [3] Z.L. Wang, *Nano Today* 5 (2010) 540–552.
- [4] W. Wu, L. Wang, Y. Li, F. Zhang, L. Lin, S. Niu, D. Chenet, X. Zhang, Y. Hao, T.F. Heinz, *Nature* 514 (2014) 470–474.
- [5] W. Wu, X. Wen, Z.L. Wang, *Science* 340 (2013) 952–957.

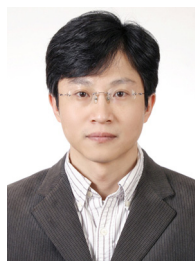
- [6] W. Wu, C. Pan, Y. Zhang, X. Wen, Z.L. Wang, *Nano Today* 8 (2013) 619–642.
- [7] R. Bao, C. Wang, Z. Peng, C. Ma, L. Dong, C. Pan, *ACS Photon* 4 (2017) 1344–1349.
- [8] J. Zhou, P. Fei, Y. Gu, W. Mai, Y. Gao, R. Yang, G. Bao, Z.L. Wang, *Nano Lett.* 8 (2008) 3973–3977.
- [9] W. Han, Y. Zhou, Y. Zhang, C.Y. Chen, L. Lin, X. Wang, S. Wang, Z.L. Wang, *ACS Nano* 6 (2012) 3760–3766.
- [10] W. Wu, Z.L. Wang, *Nano Lett.* 11 (2011) 2779–2785.
- [11] Q. Sun, W. Seung, B.J. Kim, S. Seo, S.W. Kim, J.H. Cho, *Adv. Mater.* 27 (2015) 3411–3471.
- [12] Q. Sun, D.H. Ho, Y. Choi, C. Pan, D.H. Kim, Z.L. Wang, J.H. Cho, *ACS Nano* 10 (2016) 11037–11043.
- [13] R. Yu, L. Dong, C. Pan, S. Niu, H. Liu, W. Liu, S. Chua, D. Chi, Z.L. Wang, *Adv. Mater.* 24 (2012) 3532–3537.
- [14] R. Yu, W. Wu, Y. Ding, Z.L. Wang, *ACS Nano* 7 (2013) 6403–6409.
- [15] C. Pan, R. Yu, S. Niu, G. Zhu, Z.L. Wang, *ACS Nano* 7 (2013) 1803–1810.
- [16] C. Pan, L. Dong, G. Zhu, S. Niu, R. Yu, Q. Yang, Y. Liu, Z.L. Wang, *Nat. Photon.* 7 (2013) 752–758.
- [17] M. Peng, Z. Li, C. Liu, Q. Zheng, X. Shi, M. Song, Y. Zhang, S. Du, J. Zhai, Z.L. Wang, *ACS Nano* 9 (2015) 3143–3150.
- [18] A.K. Geim, K.S. Novoselov, *Nat. Mater.* 6 (2007) 183–191.
- [19] M.J. Allen, V.C. Tung, R.B. Kaner, *Chem. Rev.* 110 (2010) 132–145.
- [20] Y. Zhang, L. Zhang, C. Zhou, *Acc. Chem. Res.* 46 (2013) 2329–2339.
- [21] G.K. Zhao, X.M. Li, M.R. Huang, Z. Zhen, Y.J. Zhong, Q. Chen, X.L. Zhao, Y.J. He, R.R. Hu, T.T. Yang, R.J. Zhang, C.L. Li, J. Kong, J.B. Xu, R.S. Ruoff, H.W. Zhu, *Chem. Soc. Rev.* 46 (2017) 4417–4449.
- [22] S.S. Lin, Y.H. Lu, J. Xu, S.R. Feng, J.F. Li, *Nano Energy* 40 (2017) 122–148.
- [23] C. Xie, L. Wang, Z.X. Zhang, D. Wang, L.B. Luo, *Nano Today* (2018), <http://dx.doi.org/10.1016/j.nanoen.2018.02.009>.
- [24] Y.J. Yu, Y. Zhao, S. Ryu, L.E. Brus, K.S. Kim, P. Kim, *Nano Lett.* 9 (2009) 3430–3434.
- [25] Y. Shi, K.K. Kim, A. Reina, M. Hofmann, L.J. Li, J. Kong, *ACS Nano* 4 (2010) 2689–2694.
- [26] H. Yang, J. Heo, S. Park, H.J. Song, D.H. Seo, K.E. Byun, P. Kim, I. Yoo, H.J. Chung, K. Kim, *Science* 336 (2012) 1140–1143.
- [27] W.J. Yu, Y. Liu, H. Zhou, A. Yin, Z. Li, Y. Huang, X. Duan, *Nat. Nanotechnol.* 8 (2013) 952–958.
- [28] W.J. Yu, L. Zheng, H. Zhou, C. Yu, W. Yang, H. Yu, X. Duan, *Nat. Mater.* 12 (2013) 246–252.
- [29] J.H. Cho, J. Lee, Y. Xia, B.S. Kim, Y. He, M.J. Renn, T.P. Lodge, C.D. Frisbie, *Nat. Mater.* 7 (2008) 900–906.
- [30] Q. Sun, D.H. Kim, S.S. Park, N.Y. Lee, Y. Zhang, J.H. Lee, K. Cho, J.H. Cho, *Adv. Mater.* 26 (2014) 4735–4740.
- [31] B.J. Kim, S.K. Lee, M.S. Kang, J.H. Ahn, J.H. Cho, *ACS Nano* 6 (2012) 8646–8651.
- [32] Y. Choi, J. Kang, D. Jariwala, M.S. Kang, T.J. Marks, M.C. Hersam, J.H. Cho, *Adv. Mater.* 28 (2016) 3742–3748.
- [33] L. Yan, C. Punckt, I.A. Aksay, W. Mertin, G. Bacher, *Nano Lett.* 11 (2011) 3543–3549.
- [34] R. Wang, S. Wang, D. Zhang, Z. Li, Y. Fang, X. Qiu, *ACS Nano* 5 (2011) 408–412.
- [35] L. Zhang, S.S. Roy, C.R. English, R.J. Hamers, M.S. Arnold, T.L. Andrew, *ACS Nano* 9 (2015) 2510–2517.
- [36] L. Collins, S. Jesse, J.I. Kilpatrick, A. Tselev, O. Varennyk, M.B. Okatan, S.A. Weber, A. Kumar, N. Balke, S.V. Kalinin, *Nat. Commun.* 5 (2014) 3871.
- [37] M. Nonnenmacher, M.P. O’Boyle, H.K. Wickramasinghe, *Appl. Phys. Lett.* 58 (1991) 2921–2923.
- [38] Y.H. Kim, J.S. Heo, T.H. Kim, S. Park, M.H. Yoon, J. Kim, M.S. Oh, G.R. Yi, Y.Y. Noh, S.K. Park, *Nature* 489 (2012) 128–132.
- [39] J.H. Kim, S.H. Hong, K.D. Seong, S. Seo, *Adv. Funct. Mater.* 24 (2014) 2404–2408.
- [40] B.J. Kim, H. Jang, S.K. Lee, B.H. Hong, J.H. Ahn, J.H. Cho, *Nano Lett.* 10 (2010) 3464–3466.



Seongchan Kim received his BS in Advanced Materials Science and Engineering from Sungkyunkwan University (SKKU) in 2016. Now he is M.Sc.-Ph.D combined student in Jeong Ho Cho’s group at SKKU Advanced Institute of Nanotechnology (SAINT) from Sungkyunkwan University (SKKU). His research interest include vertically stacked Schottky barrier transistors and its application.



Young Jin Choi received his BS in chemical engineering from Sungkyunkwan University (SKKU) in 2015. Now he is Ph.D candidate in Jeong Ho Cho's group at SKKU Advanced Institute of Nanotechnology (SAINT) from Sungkyunkwan University (SKKU). His research interest include graphene based heterojunction devices and its optoelectronic application.



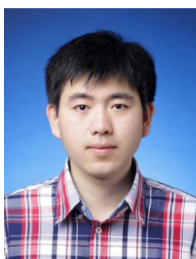
Prof. Young Jae Song received his Ph.D of Physics from Seoul National University (SNU), Seoul, Korea in 2006. And then he worked as a postdoctoral researcher in National Institute of Standards and Technology (NIST), MD, USA from 2006 to 2011, where he constructed ultra-low temperature scanning tunneling microscope (ULT STM) with a high magnetic field of 15 T and studied the electronic structures of graphene grown on SiC in atomic scale. He also worked in Samsung Advanced Institute of Technology (SAIT) and then moved to SKKU as a professor. His research works have been dedicated to the measurements of various physical properties based on AFM in nano scale or STM in atomic scale.



Hwi Je Woo received his B.Sc. of Physics from Sungkyunkwan University (SKKU), and joined Atomic Research of Nanomaterials (ARON) Lab in SKK Advanced Institute of Nano Technology (SAINT), SKKU as a M.Sc.-Ph.D combined student. His major research area is scanning probe microscopic measurements of various nanomaterials, *i.e.*, atomic force microscopy (AFM), Kelvin probe force microscopy (KPFM), magnetic force microscopy (MFM) and scattering near-field optical microscopy (sNSOM).



Prof. Zhong Lin Wang received his Ph.D from Arizona State University in physics. He now is the Hightower Chair in Materials Science and Engineering, Regents' Professor, Engineering Distinguished Professor and Director, Center for Nanostructure Characterization, at Georgia Tech. Dr. Wang has made original and innovative contributions to the synthesis, discovery, characterization and understanding of fundamental physical properties of oxide nanobelts and nanowires, as well as applications of nanowires in energy sciences, electronics, optoelectronics and biological science. His discovery and breakthroughs in developing nanogenerators established the principle and technological road map for harvesting mechanical energy from environment and biological systems for powering a personal electronics. His research on self-powered nanosystems has inspired the worldwide effort in academia and industry for studying energy for micro-nano-systems, which is now a distinct disciplinary in energy research and future sensor networks. He coined and pioneered the field of piezotronics and piezophotonics by introducing piezoelectric potential gated charge transport process in fabricating new electronic and optoelectronic devices. Details can be found at: www.nanoscience.gatech.edu.



Prof. Qijun Sun received his Ph.D from Gachon University in 2013. After that, he worked as a postdoctoral researcher in POSTECH (2013) and SKKU (2014). In 2015, he worked in Sungkyunkwan University as a research professor. From 2016, he joined Beijing Institute of Nanoenergy and Nanosystems (Chinese Academy of Sciences), as the principal investigator of Functional Soft Electronics Lab. The Main research interests of his group include graphene device based E-skin, organic electronic device, graphene electronics, printing electronics, micro-nano fabrication and transparent conducting films, aim to develop advanced systems for human health monitoring and human-machine interface.



Prof. Jeong Ho Cho obtained his BS in chemical engineering from Sogang University in 2001 and his MS and Ph.D in chemical engineering from POSTECH in 2006. He was a postdoctoral researcher in Department of Chemical Engineering and Materials Science at University of Minnesota (2006–2008) and then joined the faculty at Soongsil University in 2008. He now is an associate professor at Sungkyunkwan University (SKKU) with an appointment in SKKU Advanced Institute of Nanotechnology (SAINT) & Department of Nano Engineering. His research interests include organic electronic devices (transistor, memory, sensor) and 2-dimensional nanomaterials.



Prof. Sungjoon Lee obtained his Ph.D in electrical engineering from University of Texas at Austin in 2002. He was a researcher in Samsung Electro-mechanics R&D center (1989–1998) and Japan National Institute of AIST (Advanced Industrial Science and Technology) (2002–2003). He joined the faculty at National University of Singapore in 2003. He now is a professor at Sungkyunkwan University (SKKU) with an appointment in SKKU Advanced Institute of Nanotechnology (SAINT) & Department of Nano Engineering. His research interests include 2-dimensional nanomaterials and devices.



Prof. Moon Sung Kang received the B.S. degree in Chemical and Biological Engineering from Seoul National University, Seoul, Korea, in 2006 and the Ph.D. degree in Chemical Engineering from the University of Minnesota, Minneapolis, in 2011. In 2012, he joined the Soongsil University, Korea, in the Department of Chemical Engineering and is currently an associate professor in the department. His research focuses on fabrication and characterization of thin-film transistors and light-emitting devices and understanding electronic processes in semiconductor thin films.